SUPER-RESOLUTION ULTRAWIDEBAND ULTRASOUND IMAGING USING FOCUSED FREQUENCY TIME REVERSAL MUSIC

Foroohar Foroozan and Parastoo Sadeghi***

*InnoMind Technology, Toronto, Canada, **Research School of Engineering, Australian National University, Canberra, Australia

ABSTRACT

We propose a super-resolution image reconstruction method which uses focused frequency time reversal (FFTR) matrices to focus in frequency for ultrawideband (UWB) ultrasound signals, as well as time reversal MUltiple SIgnal Classification (MUSIC) algorithm to focus spatially on the target location. Our combined method, which we refer to as FFTR-MUSIC, is motivated by the pressing need to improve the resolution of diagnostic ultrasound systems. Compared with the TR matched filter (TRMF) and incoherent TR-MUSIC approaches, our proposed method has lower computational complexity, higher visibility, higher robustness against noise, and higher accuracy for imaging point targets when the targets are closely located. Our simulation results show that under mild speckle and noise conditions, the FFTR-MUSIC can resolve objects less than 200 μm.

Index Terms— Time Reversal, MUSIC, Ultrasound Imaging, UWB, Focusing Frequency Matrices.

1. INTRODUCTION

The clinical environment has changed. Physicians expect faster, detailed understanding of organ functions to deliver effective patient therapy. Ultrasound is an imaging modality that is relatively cheap, risk-free, and portable. But in some applications, the resolution of ultrasound images is very low. For example, ultrasound brain vascular imaging has not been clinically achieved yet due to spatial resolution limitation in ultrasound propagation through the human skull. The time reversal (TR) method utilizes the reciprocity of wave propagation in a time-invariant medium to localize an object with higher resolution. The focusing quality in the time-reversal method is decided by the size of the effective aperture of transmitter-receiver array. This effective aperture includes the physical size of the array and the effect of the environment. A complicated background will create the so-called multipath effect and can significantly increase the effective aperture size. Indeed, TR harnesses multipathing to enhance focusing resolution beyond the classical diffraction limit. This feature is known as super-resolution and is attractive for many applications such as radar [1, 2], and ultrasound imaging [3].

TR-based imaging methods use the eigenstructure of the TR matrix to image the targets. Generally, the singular value decomposition (SVD) of the TR matrix is required for each frequency bin and for each *space-space* TR-matrix. For ultrawideband (UWB) imaging, all the SVDs of *space-space* TR matrices are utilized and combined to form the final image [4]. There are two problems with this configuration: (i) the computational complexity of repeating the SVD of the TR matrix in each frequency bin is high and (ii) at each frequency, the singular vectors have an arbitrary and frequency-dependent phase resulted from the SVD. In case of DORT [5], these arbitrary phases make the eigenvectors in time domain incoherent and a pre-processing step is needed to apply the coherent signals in the back propagation phase [6]. Yavuz et. al [4, 7] proposed to use

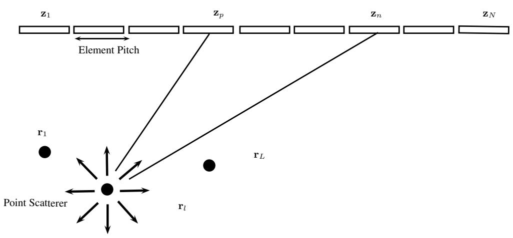

Fig. 1. Transducer array geometry with respect to the point targets in a homogeneous medium [11].

space-frequency matrices in order to overcome this difficulty, but still the computational complexity of their algorithm is high due to formation of the image using the eigenstructure of the full *space-frequency* matrices. In UWB TR-MUSIC, only the magnitude of the inner products are combined along the bandwidth and these arbitrary phases cancel out, therefore, the problem of incoherency does not exist for non-noisy data [8]. However, the super-resolution property of TR-MUSIC disappears as the signals become noisy which is due to the random phase structure induced by noise. A modified version of TR-MUSIC, PC-MUSIC [9] uses a re-formulation of TR-MUSIC which retains the phase information but also applies averaging of the pseudospectrum in frequency to cancel out the random phase degradation of TR-MUSIC in case of noisy data. The problem with PC-MUSIC is that since it uses phase information but disregards the phase response of the transducers, its ability to localize the targets at their true locations is adversely impacted [10]. A modification to PC-MUSIC was proposed in [10] to compensate the transducer phase response by developing an experimental method to estimate the phase responses beforehand. The computational complexity of this modification is still high as the SVD is needed for each frequency bin across the bandwidth and the image is formed by averaging all these pseudospectrums for each point in the region-of-interest (ROI). Also, the efficiency of this incoherent approach depends on the SNRs of the individual frequency bins.

In this paper, we propose focused frequency TR-MUSIC (FFTR-MUSIC), where we use TR-MUSIC in conjunction with TR-based frequency focusing matrices to reduce the computational complexity of incoherent TR-MUSIC as well as phase ambiguity of the PC-MUSIC in a noisy ultrasound environment. In FFTR-MUSIC, the SVD is applied once into a focused frequency TR matrix through finding unitary focusing matrices and applying a weighted averaging of the focused TR matrix over the entire bandwidth. This averaging reduces the effect of noise in *space-space* FFTR-MUSIC since the signal subspace is used after focusing in frequency. Also, after forming the FFTR matrix, the signal and noise subspaces are used once in forming the pseudospectrum which peaks at the locations of the point targets. Frequency matrices were proposed originally

978-1-4673-6997-8/15/$31.00 ©2015 IEEE

in [12, 13] for finding the direction-of-arrival of multiple wideband sources using passive arrays. Li et. al [14] modified these matrices to be used in active arrays with robust Capon beamformers in ultrasound imaging. The FFTR-MUSIC uses the TR focusing both in time and space to achieve high temporal and spatial resolution. The background Green's function at *only* the focused frequency is used as the steering vector to form the final image. This method reduces the effect of noise on target localization accuracy as well as the computational complexity needed for subspace-based methods for UWB ultrasound data by using frequency focusing matrices together with the focused frequency Green's function. Effectively, the maximum resolution achieved by the FFTR-MUSIC is only inherently limited by the SNR and the bandwidth of the transducers.

2. PROBLEM SETUP

Consider an active array of N transducer elements located at $\mathbf{z}_i$ (for $1 \le i \le N$) sonicates the medium considered in Fig. 1 and the backscattered signals are collected by the same transducer array. By employing the point target model (L point targets located at $\mathbf{r}_l$ for $1 \le l \le L$) and ignoring the multiple scattering effects between the targets, the full response matrix $\mathbf{K}(\omega)$ is formed as follows.

$$\mathbf{K}(\omega) = F(\omega) \sum_{l=1}^{L} \tau_l \mathbf{g}(\omega, r_l)\mathbf{g}^T(\omega, r_l) + \mathbf{v}(\omega), \tag{1}$$

where $F(\omega)$ represents the frequency dependency of the point scatterers, the transfer function of the probing signal and the electromechanical impulse response of the transducer elements (assuming here to be the same) and τ_l is the l'th target scattering strength. The notation $\mathbf{g}(\omega, \mathbf{r}_l) = e^{(i\phi(\omega))/2}[G(\mathbf{z}_1, \mathbf{r}_l, \omega), \cdots, G(\mathbf{z}_N, \mathbf{r}_l, \omega)]^T$ is the array steering vector with $\phi(\omega)$ being the frequency dependent phase response of the transducer and $G(\mathbf{z}_i, \mathbf{r}_l, \omega)$ is related to the medium Green's function from scatterer l to the ith transducer element shown in Fig. 1. Note that $\mathbf{K}(\omega)$ in Eq. (1) also contains an additive noise term denoted by $\mathbf{v}(\omega)$. Elaborating further on $G(\mathbf{z}_i, r_l, \omega)$ which is the integral of the medium Green's function over the surface of the transducer elements (assuming uniformly excited planar elements) [10], we have

$$G(\mathbf{z}_i, \mathbf{r}_l, \omega) = \int\int_{S_i} \frac{e^{-j\tilde{k}|\mathbf{r}_l - \mathbf{z}_i|}}{4\pi|\mathbf{r}_l - \mathbf{z}_i|}\, dS, \tag{2}$$

where $\tilde{k} = (\omega/c) - i\alpha$, with c being the sound propagation speed and α is the amplitude of the attenuation coefficient of the medium. Using linear algebra and for point targets, it is straightforward to show that the rank R of matrix $\mathbf{K}(\omega)$ is equal to the dimension of the vector space $\mathcal{G} \subseteq C^N$ spanned by the Green's function vectors, i.e. $\mathbf{g}(\omega, \mathbf{r}_l)$ [15, 16]. The singular value decomposition (SVD) of the matrix $\mathbf{K}$ is expressed as follows

$$\mathbf{K}(\omega) : C^N \to C^N \qquad \mathbf{K}(\omega)\mathbf{v_i}(\omega) = \lambda_i \mathbf{u}_i(\omega) \tag{3}$$

where $\mathbf{u}_i$, $\mathbf{v}_i$ and λ_i are, respectively, the left-singular vectors, right-singular vectors, and singular values of matrix $\mathbf{K}(\omega)$. Since rank R equals the dimension of the vector space spanned by the Green's function vectors $\mathbf{g}(\omega, \mathbf{r}_l)$, for $(1 \le l \le L)$, therefore, R also equals the number of targets L if $(L < N)$. This analysis of $\mathbf{K}(\omega)$ will be helpful in eigenstructure analysis of the TR matrix in Section 3.

3. FFTR-MUSIC IMAGING

The TR matrix [17], is defined as

$$\mathbf{T} = \mathbf{K}^H\mathbf{K} = \mathbf{V}\Lambda^H\mathbf{U}^H\mathbf{U}\Lambda\mathbf{V}^H = \mathbf{V}(\Lambda^H\Lambda)\mathbf{V}^H, \tag{4}$$

where Λ is a diagonal matrix consisting of the singular values of the full response matrix along its diagonal, and the unitary matrices $\mathbf{U}$ and $\mathbf{V}$ are formed by the left and right singular vectors, respectively. A direct result from Eq. (4) is that non-zero eigenvalues of the TR matrix are equal to the squared magnitude of the non-zero singular values of $\mathbf{K}$. Furthermore, the columns of $\mathbf{V}$ (right singular vectors of $\mathbf{K}$) are also eigenvectors of $\mathbf{T}$. Substituting the value of $\mathbf{K}$ from Eq. (1), it is straightforward to derive the structure of $\mathbf{T}(\omega)$ as

$$\mathbf{T}(\omega) = |F(\omega)|^2 \sum_{l=1}^{L}\sum_{l'=1}^{L} \Sigma_{l,l'}\mathbf{g}^*(\omega, r_l)\mathbf{g}^T(\omega, r_{l'}) + \mathbf{w}(\omega). \tag{5}$$

The term $\Sigma_{l,l'} = \tau_l{}^*\tau_{l'} < \mathbf{g}(\omega, r_l), \mathbf{g}(\omega, r_{l'}) >$ is referred to as the Coherent Point Spread Function (CPSF) and has a large impact on lateral and axial resolution of TR-based imaging algorithms. The notation $\mathbf{w}(\omega)$ represents the noise term in the TR stage. The wavefield generated from the transducer array when excited by one of the eigenvectors of the TR matrix focuses on the associated target [18] when the targets are well-resolved. Therefore, if the Green's function of the medium in which the targets are embedded is known, synthetic images highlighting the target locations can be computed. Devaney [19] showed that if targets are not well resolved, still the TR-MUSIC peaks at the locations of the scatterers, provided that the noise is relatively low.

3.1. Incoherent TR MUSIC Imaging

TR-MUSIC was originally proposed for narrowband signals and later was devised to be applied into wideband signals as well. However, the modification was essentially to transform the the frequency band into small frequency bins such that the *space-space* TR-MUSIC can be applied to each frequency bin. The pseudo-spectrum $\mathbf{A}(\omega_q, \mathbf{r})$ for Q frequency bins (ω_q for $0 \le q \le (Q-1)$) of an arbitrary observation point $\mathbf{r}$ is defined as [10]

$$\mathbf{A}(\omega_q, \mathbf{r}) = \frac{\mathbf{g}^H(\omega_q, \mathbf{r})\mathbf{U}_{\mathrm{Sig}}(\omega_q)\mathbf{U}_{\mathrm{Sig}}^H(\omega_q)\mathbf{g}^*(\omega_q, \mathbf{r})}{||\mathbf{g}(\omega_q, \mathbf{r})||^2}, \tag{6}$$

where $\mathbf{U}_{\mathrm{Sig}}(\omega_q) = [\mathbf{u}_1, \cdots, \mathbf{u}_L]$ is the signal subspace matrix. Then, the TR-MUSIC image is given as

$$\mathbf{I}(\mathbf{r}) = \frac{1}{1 - (1/Q)\sum_q \mathbf{A}(\omega_q, \mathbf{r})}. \tag{7}$$

As it is clear from (6), the $\mathbf{A}$ operator disregards the phase information in $\mathbf{U}_{\mathrm{Sig}}(\omega_q)$ when there is no noise. But in noisy data, the phases do not cancel out and the super-resolution property of TR-MUSIC is compromised.

3.2. Coherent FFTR MUSIC Imaging

Here, we apply a coherent method using the concept of focusing matrices originally proposed in [12, 14] in conjunction with the TR-MUSIC. This method involves focusing matrices to transform the time reversal operator at different frequency bins onto a single reference frequency and a coherent focused time reversal operator is achieved. The reference frequency is assumed to be ω_0 and the unitary focusing matrices [12] for Q frequency bins (ω_q for $0 \le q \le (Q-1)$) are to be found. These unitary matrices $\mathbf{B}(\omega_q)$ minimize the difference between $\mathbf{T}(\omega_0)$ and the transformed TR matrix at frequency q with the following minimization problem.

$$\min_{\mathbf{B}(\omega_q)} \|\mathbf{K}^H(\omega_0) - \mathbf{B}(\omega_q)\mathbf{K}^H(\omega_q)\|_F \tag{8}$$
$$\text{subject to} \quad \mathbf{B}^H(\omega_q)\mathbf{B}(\omega_q) = \mathbf{I},$$

where $\|.\|_F$ denotes the Frobenius matrix norm. Applying SVD on $\mathbf{K}^H(\omega_q)\mathbf{K}(\omega_0)$, it has been shown in [12] that the solution to the problem (8) is given by

$$\mathbf{B}(\omega_q) = \mathbf{V}(\omega_q)\mathbf{U}^H(\omega_q), \tag{9}$$

where $\mathbf{V}(\omega_q)$ and $\mathbf{U}(\omega_q)$ are the right and left eigenvalues of the TR matrix $\mathbf{K}^H(\omega_q)\mathbf{K}(\omega_0)$. Then, the coherently focused TR operator is the weighted average of the transformed matrix of TR with unitary matrix $\mathbf{B}(\omega_q)$ as follows

$$\tilde{\mathbf{T}}(\omega_0) = \sum_{q=0}^{(Q-1)} \beta_q \mathbf{B}(\omega_q)\mathbf{T}(\omega_q)\mathbf{B}^H(\omega_q), \tag{10}$$

where β_q is the qth weight proportional to the SNR of the this frequency bin. In summary, we first use the TR matrix to focus on frequency and then by using the focused TR matrix, we apply the TR-MUSIC to focus spatially on the scatterers. The advantage with this approach is that only the Green's function at the focused frequency is needed for image formation. It is worth noting that for incoherent TR-MUSIC and PC-MUSIC, the array steering vector should be computed for each frequency bin over the entire grid. The final step will be to form the pseudospectrum of FFTR-MUSIC as follows.

$$\mathbf{A}(\omega_0, \mathbf{r}) = \frac{\mathbf{g}^H(\omega_0, \mathbf{r})\mathbf{U}_{\mathrm{Sig}}(\omega_0)\mathbf{U}_{\mathrm{Sig}}^H(\omega_0)\mathbf{g}^*(\omega_0, \mathbf{r})}{\|\mathbf{g}(\omega_0, \mathbf{r})\|^2}, \tag{11}$$

where $\mathbf{U}_{\mathrm{Sig}}(\omega_0)$ is the signal subspace matrix at the focused frequency resulted from the SVD of $\tilde{\mathbf{T}}(\omega_0)$. Finally, the FFTR-MUSIC image is given by

$$\mathbf{I}(\mathbf{r}) = \frac{1}{1 - \mathbf{A}(\omega_0, \mathbf{r})}. \tag{12}$$

4. SIMULATIONS

In this section, we demonstrate the performance of our proposed method FFTR-MUSIC for imaging point targets embedded in a low speckle noise environment using several simulated examples. Field II simulator [20] is used to generate acoustic wave fields and to simulate impulse responses of transducers. The first example consists of a medium of random point scatterers and two closely located targets at (0, 37)mm and (1, 38)mm (2λ apart, and $\tau_1 = 90$, $\tau_2 = 100$) using a 128-transducer linear array with a kerf of 0.05mm, width of 0.4mm, and height of 5mm. A sinusoidal probing signal at centre frequency of 3 MHz is sonicating the low speckle medium with sound speed of 1540 m/s (the wavelength λ is 440 micron) and an ultrasound attenuation coefficient α of 0.3 dB/cmMHz. The ROI is devided into 101 $\times$ 201 points with the grid size of 10 μm. We record the full matrix of 128 $\times$ 128 RF-data with a sampling frequency of 100 MHz to apply the TR imaging algorithms. A white noise is added to each of the signals with a SNR of 10dB. To form the steering array of the medium, we follow the model given in Eq. (2) and use the phase of the transducers at the focused frequency.

We move the point target laterally close to each other at λ and $\lambda/2$ to validate the resolvability of the targets in a noisy environment using our proposed method. Fig. 2 shows the images of the point scatterers when the TRMF, incoherent TR-MUSIC, and FFTR-MUSIC methods are applied to the response matrix. When the targets are 2λ apart, all the three TR-based imaging algorithms can resolve the two targets, but the resolution is much better with FFTR-MUSIC approach with much less sidelobes and focused main lobe.

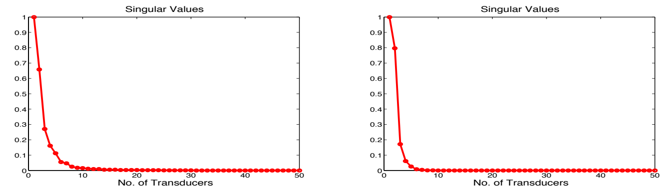

(a) (b)

Fig. 3. Normalized singular values of the TR matrix; the targets are $\lambda/2$ apart at: (a) Center frequency; (b) TR focused frequency.

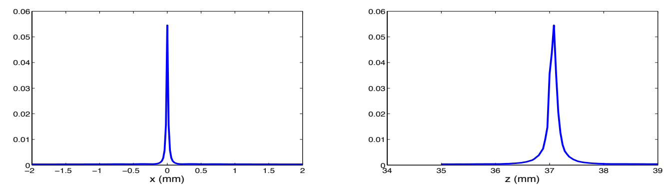

(a) (b)

Fig. 4. CPSF of a point source at (0, 37) mm (a) x- (b) z-profiles.

When the distance between the point targets are λ, still all the TR-based imaging techniques can localize the targets while the FFTR-MUSIC provides the best resolution. As the targets become $\lambda/2$ apart, neither the TRMF nor the incoherent TR-MUSIC are able to resolve the targets in lateral direction as shown in Fig. 2 ((g)-(i)). In this case, the FFTR-MUSIC can still resolve the targets with high resolution. Figure 2 ((j)-(l)) plots the x-profile of the FFTR-MUSIC images when the targets are $\lambda/2$ apart and it shows that the visibility of the targets in lateral direction is very good compared to the other approaches. For this scenario, the normalized singular values of the incoherent TR-MUSIC approach at the centre frequency and the one of the FFTR-MUSIC matrix is plotted in Fig. 3. It is clear that in the presence of noise, the FFTR-MUSIC approach could estimate the signal subspace rank with higher accuracy. However, all the images suffer from the so-called elongation artifact in axial direction and this is due to the limitation of the 1D linear array systems to resolve the targets in axial direction. When we plot the CPSF of this setup using a single point scatterer as shown in Fig. 4 , it can be seen that the lateral and axial resolution is much different due to the limitation of the linear array. Our further investigations (removed here due to the lack of space) show that maximum resolution achieved by the FFTR-MUSIC is only inherently limited by the SNR and bandwidth of the transducers.

5. SUMMARY

Motivated by the need to substantially improve the resolution of ultrasound imaging, the paper suggested that the eigenstructure of TR focused frequency matrix can improve the resolution, resolvability of closely point sources, and visibility of the image when there is observation noise and low speckle in the medium. The computational complexity of the proposed approach is low compared to the TRMF and incoherent TR-MUSIC due to the use of search steering vector at the focused frequency. The simulation results in Field II shows that with a linear transducer array, it is possible to resolve objects with less than 200 μm resolution in lateral direction. In our future work, we will modify this technique to localize extended targets in a high speckle environment with real ultrasound data.

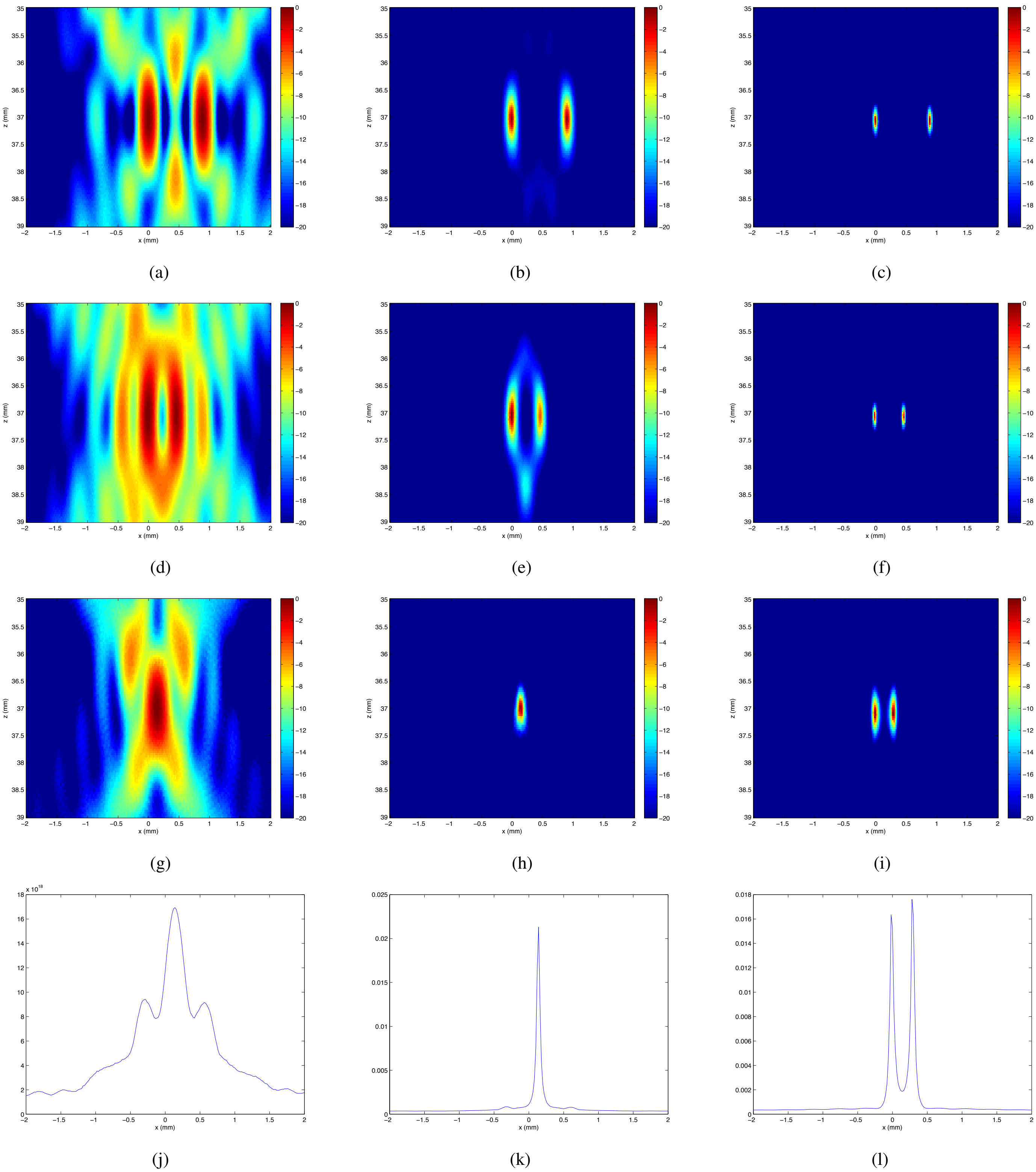

Fig. 2. TR-based imaging results for 2 point targets in a low speckle noise medium with SNR = 10 dB and 20 dB display dynamic range: (a)-(c) The point targets are 2λ apart; (d)-(f) The point targets are λ apart; (g)-(i) The point targets are $\lambda/2$ apart. The left column images are resulted from the TRMF; the middle column images are based on incoherent TR-MUSIC and the right column images are resulted from the FFTR-MUSIC. Subplots (j)-(l) show the x-profiles of the images plotted in (g)-(i).

6. REFERENCES

[1] F. Foroozan and A. Asif, "Time reversal based active array source localization," *IEEE Trans. on Signal Processing*, vol. 59, no. 6, pp. 2655 –2668, June 2011.

[2] ——, "Cramér-Rao bound for time reversal active array direction of arrival estimators in multipath environments," *Proceedings of the International Conference on Acoustics, Speech, and Signal Processing (ICASSP)*, pp. 2646–2649, Mar. 2010.

[3] M. Fink, C. Prada, F. Wu, and D. Cassereau, "Self focusing in inhomogeneous media with time reversal acoustic mirrors," *IEEE Proceedings of Ultrasonics Symposium*, pp. 681–686 vol.2, Oct 1989.

[4] M. Yavuz and F. Teixeira, "Frequency dispersion compensation in time reversal techniques for UWB electromagnetic waves," *IEEE Geoscience and Remote Sensing Letters*, vol. 2, no. 2, pp. 233–237, April 2005.

[5] C. Prada and J. Thomas, "Experimental subwavelength localization of scatterers by decomposition of the time reversal operator interpreted as a covariance matrix," *Journal of the Acoustical Society of America*, vol. 114, pp. 235–243, 2003.

[6] M. Yavuz and F. Teixeira, "Full time-domain DORT for ultrawideband electromagnetic fields in dispersive, random inhomogeneous media," *IEEE Transactions on Antennas and Propagation*, vol. 54, no. 8, pp. 2305–2315, Aug. 2006.

[7] ——, "A numerical study of time-reversed UWB electromagnetic waves in continuous random media," *IEEE Antennas and Wireless Propagation Letters*, vol. 4, pp. 43–46, 2005.

[8] M. E. Yavuz, "Time reversal based signal processing techniques: algorithms and applications on ultrawideband electromagnetic remote sensing," Ph.D. dissertation, The Ohio State University, 2008.

[9] E. G. Asgedom, L.-J. Gelius, A. Austeng, S. Holm, and M. Tygel, "Time-reversal multiple signal classification in case of noise: A phase-coherent approach," *The Journal of the Acoustical Society of America*, vol. 130, no. 4, 2011.

[10] Y. Labyed and L. Huang, "Super-resolution ultrasound imaging using a phase-coherent MUSIC method with compensation for the phase response of transducer elements," *IEEE Transactions on Ultrasonics, Ferroelectrics, and Frequency Control*, vol. 60, no. 6, pp. 1048–1060, June 2013.

[11] F. Foroozan and S. Shahbazpanahi, "MUSIC-based array imaging in multi-modal ultrasonic non-destructive testing," in *Sensor Array and Multichannel Signal Processing Workshop (SAM), 2012 IEEE 7th*, June 2012, pp. 529–532.

[12] H. Hung and M. Kaveh, "Focussing matrices for coherent signal-subspace processing," *IEEE Transactions on Acoustics, Speech and Signal Processing*, vol. 36, no. 8, pp. 1272–1281, Aug 1988.

[13] H. Wang and M. Kaveh, "Coherent signal-subspace processing for the detection and estimation of angles of arrival of multiple wide-band sources," *IEEE Transactions on Acoustics, Speech and Signal Processing*, vol. 33, no. 4, pp. 823–831, Aug 1985.

[14] Z. Wang, J. Li, and R. Wu, "Time-delay- and time-reversal-based robust capon beamformers for ultrasound imaging," *IEEE Transactions on Medical Imaging*, vol. 24, no. 10, pp. 1308–1322, Oct. 2005.

[15] F. K. Gruber, E. A. Marengo, and A. J. Devaney, "Time-reversal imaging with multiple signal classification considering multiple scattering between the targets," *Journal of the Acoustical Society of America*, vol. 115, no. 6, pp. 3042–3047, 2004.

[16] A. J. Devaney, E. A. Marengo, and F. K. Gruber, "Time-reversal-based imaging and inverse scattering of multiply scattering point targets," *Journal of the Acoustical Society of America*, vol. 118, no. 5, pp. 3129–3138, 2005.

[17] C. Prada and M. Fink, "Eigenmodes of the time reversal operator: A solution to selective focusing in multiple-target media," *Wave Motion*, pp. 151–163, 1994.

[18] C. Prada, J. L. Thomas, and M. Fink, "The iterative time reversal process: analysis of the convergence," *Journal of the Acoustical Society of America*, vol. 97, pp. 62–71, 1995.

[19] A. Devaney, "Time reversal imaging of obscured targets from multistatic data," *IEEE Transactions on Antennas Propagation*, vol. 53, pp. 1600–1610, 2005.

[20] J. Jensen, "Simulation of advanced ultrasound systems using Field II," in *2004 IEEE International Symp. on Biomedical Imaging: Nano to Macro*, April 2004, pp. 636–639 Vol. 1.